J Mater Sci: Mater Med (2017) 28:191
DOI 10.1007/s10856-017-5999-z

TISSUE ENGINEERING CONSTRUCTS AND CELL SUBSTRATES

Original Research

Silk fibroin-Pellethane® cardiovascular patches: Effect of silk fibroin concentration on vascular remodeling in rat model

Pinkarn Chantawong[1] · Takashi Tanaka[1] · Akiko Uemura[1] · Kazumi Shimada[1] · Akira Higuchi[2] · Hirokazu Tajiri[2] · Kohta Sakura[2] · Tomoaki Murakami[3] · Yasumoto Nakazawa[2] · Ryou Tanaka[1]

Received: 20 March 2017 / Accepted: 24 October 2017 / Published online: 14 November 2017

Abstract Life-threatening cardiovascular anomalies require surgery for structural repair with cardiovascular patches. The biomaterial patch, derived from *Bombyx mori* silk fibroin (SF), is used as an alternative material due to its excellent tissue affinity and biocompatibility. However, SF lacks the elastomeric characteristics required for a cardiovascular patch. In order to overcome this shortcoming, we combined the thermoplastic polyurethane, Pellethane® (PU) with SF to develop an elastic biocompatible patch. Therefore, the purpose of this study was to investigate the feasibility of the blended SF/PU patch in a vascular model. Additionally, we focused on the effects of different SF concentrations in the SF/PU patch on its biological and physical properties. Three patches of different compositions (SF, SF7PU3 and SF4PU6) were created using an electrospinning method. Each patch type ($n = 18$) was implanted into rat abdominal aorta and histopathology was assessed at 1, 3, and 6 months post-implantation. The results showed that with increasing SF content the tensile strength and elasticity decreased. Histological evaluation revealed that inflammation gradually decreased in the SF7PU3 and SF patches throughout the study period. At 6 months post-implantation, the SF7PU3 patch demonstrated progressive remodeling, including significantly higher tissue infiltration, elastogenesis and endothelialization compared with SF4PU6. In conclusion, an increase of SF concentration in the SF/PU patch had effects on vascular remodeling and physical properties. Moreover, our blended patch might be an attractive alternative material that could induce the growth of a neo-artery composed of tissue present in native artery.

Graphical abstract

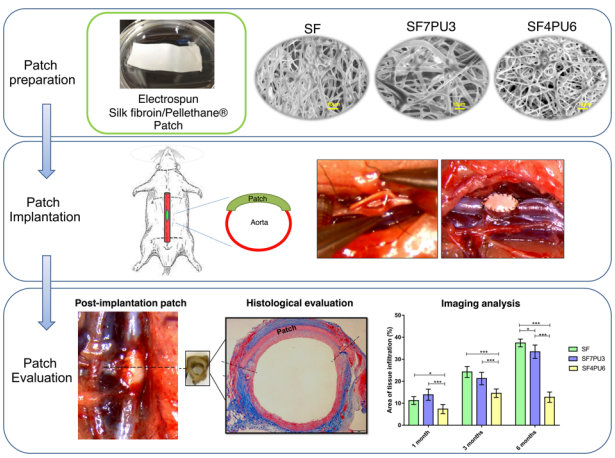

Electronic supplementary material The online version of this article (https://doi.org/10.1007/s10856-017-5999-z) contains supplementary material, which is available to authorized users.

✉ Yasumoto Nakazawa
yasumoto@cc.tuat.ac.th

✉ Ryou Tanaka
ryovet@me.com

[1] Department of Veterinary Surgery, Tokyo University of Agriculture and Technology, Fuchu, 183-8509 Tokyo, Japan

[2] Department of Biotechnology and Life Science, Tokyo University of Agriculture and Technology, Koganei, 184-8588 Tokyo, Japan

[3] Department of Veterinary Toxicology, Tokyo University of Agriculture and Technology, Fuchu, 183-8509 Tokyo, Japan

1 Introduction

Cardiovascular diseases are the most common causes of serious morbidity worldwide. Life-threatening cardiac anomalies such as atrio-ventricular septal defects and pulmonic stenosis require surgery for structural repair with cardiac patches. Various patch materials currently used for cardiovascular tissue reconstruction include prosthetic materials such as polyethylene terephthalate (PET) and polytetrafluoroethylene (PTFE), autologous pericardium and allogenic-xenogenic pericardium [1, 2]. However, these patches have several disadvantages in long-term use due to their inability to grow with patient's organ, their unsuitability for tissue remodeling, their susceptibility to thrombotic stenosis and calcification, and decline in their mechanical strength [3–5]. All these problems are caused by the use of inappropriate materials and often lead to reoperation. Therefore, alternative tissue engineered biomaterial patches for cardiovascular reconstruction are urgently required.

Silk fibroin (SF) is a natural biopolymer derived from *Bombyx mori* cocoons. Fibroin is the core filaments of silk and is composed of semicrystalline and β-sheet crystalline. The crystalline domains consist primarily of the amino acids: glycine, alanine, serine, threonine and valine [6]. The β-sheet crystal region provides the tensile strength and elasticity of the silk fiber [7]. Recently, SF is also an alternative candidate for biomaterial because of its excellent property superior to other natural biopolymers [8]. Previous study showed that SF bio-conjugated scaffold induced tissue regeneration and resisted infection during the treatment of musculoskeletal disease. It has advantages over poly (lactic acid) and collagen in biocompatibility and antigenicity [9]. Moreover, other fascinating attributes include excellent tissue affinity, biodegradability, low immunogenicity and easily accessible chemical groups for functional modifications [8, 10]. SF offers versatility in matrix scaffold design for engineering various tissues such as cornel epithelial sheet, vascular graft, bone and cartilage scaffolds [11–14]. However, the limitations of SF materials are their lack of elastomeric characteristics and of strength. Previous studies demonstrated that a nonwoven sheath prepared from SF had inadequate elasticity required for ligament scaffold [15] and that a SF vascular graft was stiffer than collagen-coated grafts for implantation [16]. In order to overcome these disadvantages, this study focused on developing an elastic biocompatible material using SF as the material base to create a novel cardiac patch.

Pellethane® (2363-80AE, DOW chemical) is a family of medical-grade thermoplastic polyurethane (PU) elastomers with a wide range of properties [17]. It is a polytetramethylene glycol based PU, which is composed of organic units joined by urethane linkages. For years, PU represented synthetic elastomer that has been applied for a variety of medical implants. It is used in the fabrication of medical devices such as cardiac pace makers and vascular grafts [18, 19]. This study used Pellethane® because it is a well-defined polymer which is easy to process by the electrospining method and has excellent hydrolytic stability. Moreover, it can be manipulated in tissue-engineering scaffolds due to its high elasticity and has good blood compatibility and resistance to microorganisms [20–22]. A previous study demonstrated that porous Pellethane® vascular graft provided an appropriate scaffold for cell attachment, host cell ingrowth and matrix deposition. It showed successful reconstruction of the host vessel within 6 months [23].

Recently, there has been great interest in modification of a polymeric material such as PU with natural SF. In 2003, SF-coated poly(carbonate) urethane membranes were seeded with human adult fibroblasts. This modified membrane could support the adhesion and growth of fibroblasts without secreting pro-inflammatory cytokines [24]. In addition, an in vitro study of SF blended with biobased PU films in various concentrations assessed their capacity to support myoblast differentiation. A hybrid film with a high SF concentration improved cell adhesion, proliferation and myogenic activity of C2C12 (a mouse myoblast cell line). Furthermore, it provided the flexibility and biocompatibility for soft tissue reconstruction [25].

Even though SF and PU polymer combinations seem to have been successfully used as tissue scaffold in in vitro studies, little is known about their potential for use in a cardiovascular patch, especially in in vivo studies. To create the desired SF/PU patch, this study used the electrospining method to form a non-woven patch. This is an attractive technique for fabricating nanostructured vascular scaffolds with high surface area and porosity that regenerative cells can easily infiltrate. Thus, we expected that our patches should have desired features including possessing proper elasticity, maintaining tensile strength and promoting vascular remodeling. The purposes of this study were to (1) investigate the feasibility of a blended SF/PU patch in a rat vascular model and (2) evaluate the effects of different SF concentrations in blended SF/PU patches on vascular remodeling and physical properties.

2 Materials and methods

2.1 Silk fibroin/ Pellethane® patch preparation

Segmented Pellethane® was used as the PU source. To prepare silk fibroin, 250 g of *Bombyx mori* cocoons were degummed in a boiling aqueous Na2CO3 (0.02 M) solution for 30 min. After that, the degummed fibers were

thoroughly rinsed with deionized water at 40 °C and dehydrating was repeated 5 times. The silk fibers obtained were rinsed with cold water and allowed to air dry. The regenerated silk fibroin solution was dissolved in a 9 M lithium bromide solution to a concentration of 10 w/v% at 37 °C for 2 h (agitation speed 0–1.5 h for 100 rpm and 1.5–2h for 65 rpm). Then, it was dialyzed against distilled water for three days at 4 °C using a cellulose membrane (MWCO 14,000) to remove lithium bromide. The dialyzed solution was centrifuged at 4 °C and 8500 rpm for 30 min to remove impurities and insoluble matter. The final concentration of the SF aqueous solution was 4–5% (w/v). To prepare the SF sponge, an aqueous solution of SF was diluted with distilled water 1% w/v and processed by lyophilization.

The SF sponge and PU were dissolved in 1,1,1,3,3,3-Hexafluoro-2-propanol (HFIP) solution. The HFIP solutions of each combination of PU and SF were mixed in the weight ratio SF/PU = 10/0 (SF), 7/3 (SF7PU3), 4/6 (SF4PU6) (w/w) respectively and stirred by a magnetic stir bar for 12 h. After that SF/PU solutions at 6% (w/v) were loaded into the electrospinning machine (Esprayer ES2000S2A, Fuence Company, Japan). The conditions of the spinning process were as follows: temperature: 25–30 °C; relative humidity: 30–50%; distance between target and syringe top: 10 cm; discharge speed: 12 µl/min and electric voltage: 16–17 kV. The processing time for each sample was 3 h. The dimensions of the patch created were 15 mm in width, 25 mm in length and 100 µm in thickness. The thickness of the patch was measured with a micrometer (406–250, Mitutoyo Co. Ltd., Japan). In order to insolubilize the nonwoven patches, they were put in desiccators at 37 °C and 100% humidity for 24 h and then purified in water for three days. After that, all patches were sterilized in an autoclave at 121 °C for 30 min and kept in dry sterile packages until the implantation process. The final product was confirmed by 1H NMR 13 C and 13 C CP/MAS NMR analysis.

2.2 Patch morphological and physical property observations

The morphology of the electrospun patches was evaluated by a scanning electron microscope (SEM) (JSM-6510 JEOL, Japan) and the fiber diameter was measured with Image J (1.48, National Institutes of Health, USA). The diameter of 50 fibers was randomly measured from SEM images, and the average diameter and standard deviation were calculated. For the tensile strength test, representative patches in each ratio ($n = 9$) were cut into 3 mm in width and 25 mm in length segment. The edge of the specimen was held in 15 mm length between the clamps and pulled at a cross-head speed of 2 mm/min until break point and analysis. We measured the retention strength with EZ-Test (Shimadzu, Japan) in order to evaluate patch strength. Additionally, the Young's modulus was defined by the slope of the stress-strain curve for elastic assessment.

2.3 Animal study design

Healthy male Sprague-Dawley rats (Charles River Laboratories, Japan) 3–4 months old and weighing 250–350 g were used for the in vivo study. All rats were housed and maintained in micro-isolator cages at 23 ± 2°C and with a 12-h light/dark cycle. All procedures involving experimental protocols and surgeries were approved by the Animal Care and Use Committee of Tokyo University of Agriculture and Technology (TUAT) (Approval number: 28–79), and animal care was provided in accordance with the "Guide for the Care and Use of Laboratory Animals" which was established by TUAT.

2.4 Patch implantation

Three patch types (SF, SF7PU3 and SF4PU6) were prepared in an ellipse shape with 3 mm in width, 6 mm in length and 100 µm in thickness. Each type of patch was implanted the abdominal aorta of 18 rats under a stereoscopic microscope (M60, Leica Microsystems, Japan). All animals were anesthetized with intraperitoneal injection of pentobarbital (Somnopentyl®) 50 mg/kg body weight. Heparin (100IU/kg) was administered intravenously. The abdominal aorta was approached through a midline laparotomy incision. After that, the proximal and distal portions of the aorta were clamped with vascular clips and a transverse incision of the aorta was made between the clamps. Then, the patch was sutured to the cut edge of the aorta with continuous 9–0 monofilament nylon sutures (BEAR Co., Japan). After the suture was completed, the vascular clips were slowly removed and blood flow was restored through the patch. Finally, orbifloxacin (VICTAS®) 0.5 mg/kg was injected intraperitoneally before the abdomen was closed in layers with interrupted sutures of 3–0 polyglyconate (Maxon^{TM}, Covidien Co., U.S).

2.5 Histological studies

The animals were sacrificed at 1, 3 and 6 months after implantation ($n = 6$ in each group) with an intracardiac injection of KCl 0.3 mL/rat. The patches were assessed macroscopically and carefully removed together with the surrounding tissue. The patches were cut transversely into two pieces, fixed in 95% methanol for 12 h, clarified in xylene, embedded in paraffin and cut into 3-µm sections for tissue staining. For vascular remodeling evaluation, tissue sections were stained with hematoxylin and eosin (HE) for

Table 1 Histological grading criteria used to evaluate the degree of chronic inflammation, foreign body reaction, and surrounding fibroconnective tissue

Grade	Chronic inflammation	Foreign body reaction	Surrounding fibroconnective tissue
0	No visible inflammation	An absence of multinucleated giant cells	No fibroconnective tissue
1	Mild inflammation, an average of inflammatory cells fewer than 20 cells/high power field (HPF)	Mild foreign body reaction, an average of multinucleated giant cells less than 5 cells/ HPF	Minimal fibroconnective tissue around the patch
2	Moderate inflammation, an average of inflammatory cells 20–35 cells/ HPF	Moderate foreign body reaction, an average of multinucleated giant cells 5–10 cells/ HPF	Multifocal accumulation of loosely-organized fibroconnective tissue around the patch
3	Extensive inflammation, an average of inflammatory cells more than 35 cells/ HPF	Severe foreign body reaction, an average of multinucleated giant cells more than 10 cells/ HPF	Diffuse accumulation of densely-organized fibroconnective tissue around the patch

inflammation, Masson's trichrome (MTC) for collagenization, Elastica Van Gieson (EVG) for elastogenesis and Von Kossa for calcification. For immunohistochemistry, the primary antibodies used included: Iba1 (1:50, Proteintech Inc., USA), CD31 (1:50, Lifespan Biosciences Inc., USA) and alpha-smooth muscle actin (α-SMA) (1:100, Nichirei Biosciences Inc., Japan); indicating the macrophages, endothelial cells, and smooth muscle cells, respectively. Antibody binding was detected with biotinylated secondary antibody (Nichirei Biosciences Inc., Japan) and color development was performed with aminoethyl carbazole for CD31, and diaminobenzidine for α-SMA and Iba1. Finally, nuclei were counterstained with hematoxylin solution.

Histological features of the stained specimens were examined by light microscopy to evaluate the overall biological reactions to the patches. These were fundamental aspects of tissue reactions, and each histological parameter was graded from 0 to 3 [1, 26, 27]. The details of the grading criteria are provided in Table 1. Additional macroscopic and histologic examinations of the organs (heart, lung, spleen, liver and kidney) of rats of all groups were performed to evaluate the systemic toxicity of the patches after 6 months' implantation.

2.6 Imaging analysis

The tissue infiltration, elastogenesis, endothelialization and neovascular tissue thickness were analyzed from MTC, EVG, CD31 and alpha-SMA stained specimens using the image analysis software ImageJ (version 1.44; National Institute of Mental Health, Bethesda, USA) [27]. Three sections of each individual sample were measured and averaged for a total of six samples. The percentage of tissue infiltration was calculated from the area of blue collagenous fibers which migrated inside a patch and the total area of the patch. This analysis was regarded as the degree of biocompatibility [27, 28]. In this study, biocompatible evaluation focused on the ability of host cells to directly infiltrate the patch. The percentage of elastogenesis was measured from the area of dark purple elastic fibers beneath the patch and the total area of neovascular tissue. Considering that the elastogenesis is important in tissue organization process due to maintain the stability and mechanical strength of the arterial wall, this percentage could be considered as the degree of tissue organization. In the CD31-stained specimens, the extent of the area of endothelial cell coverage under the patch and the length of the stained luminal surface were measured as a percentage of endothelialization [27, 29]. The neovascular thickness was measured from the length of neotissue underneath the patch (tunica media) to the innermost layers (tunica intima) and compared with the thickness wall of six native aorta.

2.7 Statistical analysis

All data were analyzed in terms of standard error of the mean. The statistically significant differences among patch groups were defined using one-way analysis of variance, followed by the Tukey's multiple comparisons test. A Pearson correlation test was performed to determine the degree of relationship between endothelialization and tissue infiltration. Data analyses utilized the statistics GraphPad Prism software (Version 7.0, GraphPad Inc., USA). Statistical significance was considered as p-value < 0.05.

3 Result

3.1 Patches morphological and physical property observations

SEM images of patch structure are shown in Fig. 1. All patch types revealed a fine fiber structure. The SF and PU were blended within each fiber and provided porosity that regenerative cells could easily infiltrate. The average of the fiber diameters is shown in Table 2 and the highest fiber diameter was found in the SF patch.

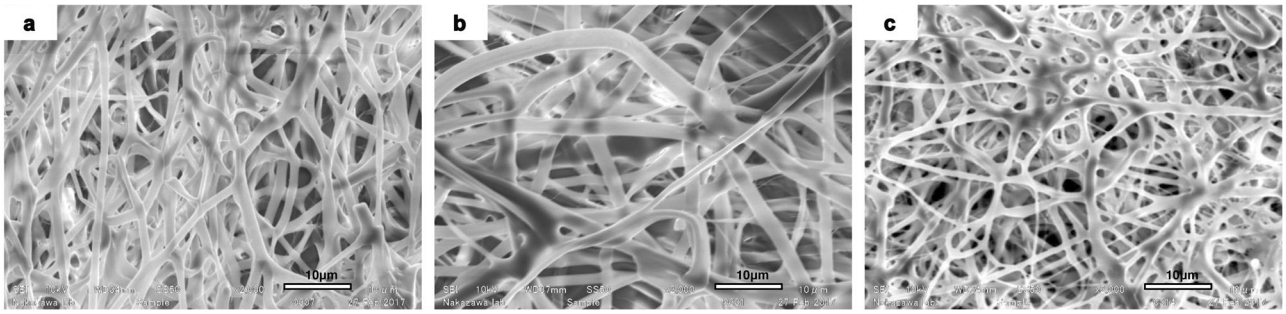

Fig. 1 SEM images show the structure of three patch types. SF **a**, SF7PU3 **b** and SF4PU6 **c**

Table 2 The average of the fiber diameters of SF and SF/PU patches (mean ± standard error, $n = 50$/patch types)

Patch types	Fiber diameters (μm)
SF	1.61 ± 0.98
SF7PU3	1.32 ± 0.78
SF4PU6	$0.94 \pm 0.44^{a,b}$

[a] Compared with SF group, $P < 0.05$

[b] Compared with SF7PU3 group, $P < 0.05$

The differences in physical properties among the three patch types were evaluated. The stress-strain curve of the patch was determined by a tensile test (Fig. 2). The Young's modulus, the ultimate tensile strength (UTS) and the strain at break were calculated from the stress-strain curves and are shown in Fig. 3a, b and c, respectively. The highest SF content patch (SF) had UTS ranging from 3.99 to 5.32 MPa, and breaking strains from 25.68–39.75%, which were lower than the lowest SF content patch (SF4PU6). With regard to Young's modulus, the SF patch had the highest values ranging from 29.47 to 33.86 MPa, and this was significant ($p < 0.001$). It can be seen that as the SF content increased, the UTS slightly decreased and the Young's modulus increased indicating the stiffness of the SF patch. In addition, the strain at break showed a significant decrease with the increase of the SF content (Fig. 3c).

3.2 Gross observations

3.2.1 Patch implantation

The SF patch was stiff and fragile when compared with the blended SF/PU patches. During the implantation, both SF/PU patch groups were impervious to blood leakage, but the SF patch showed blood oozing at the anastomosis area because it was perforated by the suture needle (Fig. 4a–c). This problem required 3–5 min of gauze pressure to obtain sufficient hemostasis. The average clamping time during implantation of the SF4PU6 and SF7PU3 patches were 14 ± 3 and 16 ± 2 min respectively, which were shorter than the time required for the SF patch (21 ± 4 min) because their elastic and flexible character made it easy to cut, handle and suture them. During the experimental period, there were no clinical complications or early postoperative deaths in any surgical group.

3.2.2 Gross observation post-implantation

At autopsy, it was consistently found that all patches were well merged with the native abdominal aorta and their surfaces were covered with connective tissue (Fig. 4d–f). After 6 months implantation, SF7PU3 and SF patches were easily isolated from surrounding organs. In contrast, the SF4PU6 patch showed moderate adhesion with adjacent abdominal organs or surrounding tissue. There was no evidence of thrombus formation in any of the patch groups.

3.3 Histopathological examination

Representative sections of each patch were assessed for biological reactions. One month post-implantation, HE staining confirmed the presence of inflammatory cells including neutrophils, lymphocytes and plasma cells in all patch groups (Supplementary Fig. 2). Macrophage cells surrounding the patch were detected from positive Iba1 staining (Supplementary Fig. 1). There was no significant difference in inflammatory response among patch groups (Table 3). However, the numbers of inflammatory cells gradually decreased in SF7PU3 and SF patches after 3 and 6 months (Supplementary Fig. 4 and Fig. 5b–d). Conversely, in the SF4PU6 patch, intense foreign body reaction was persistently observed until 6 months (Table 3).

The extracellular matrix components, including collagen and elastin, were evaluated from the neovascular tissue layer grew up until 6 months post implantation. Collagen synthesis and tissue infiltration into patches were confirmed with MTC staining. Blue fibers were indicative of collagen fibers whereas pink to red color represented muscle and cytoplasm. One month after implantation, SF7PU3 and SF4PU6 patches were surrounded by collagen. The highest

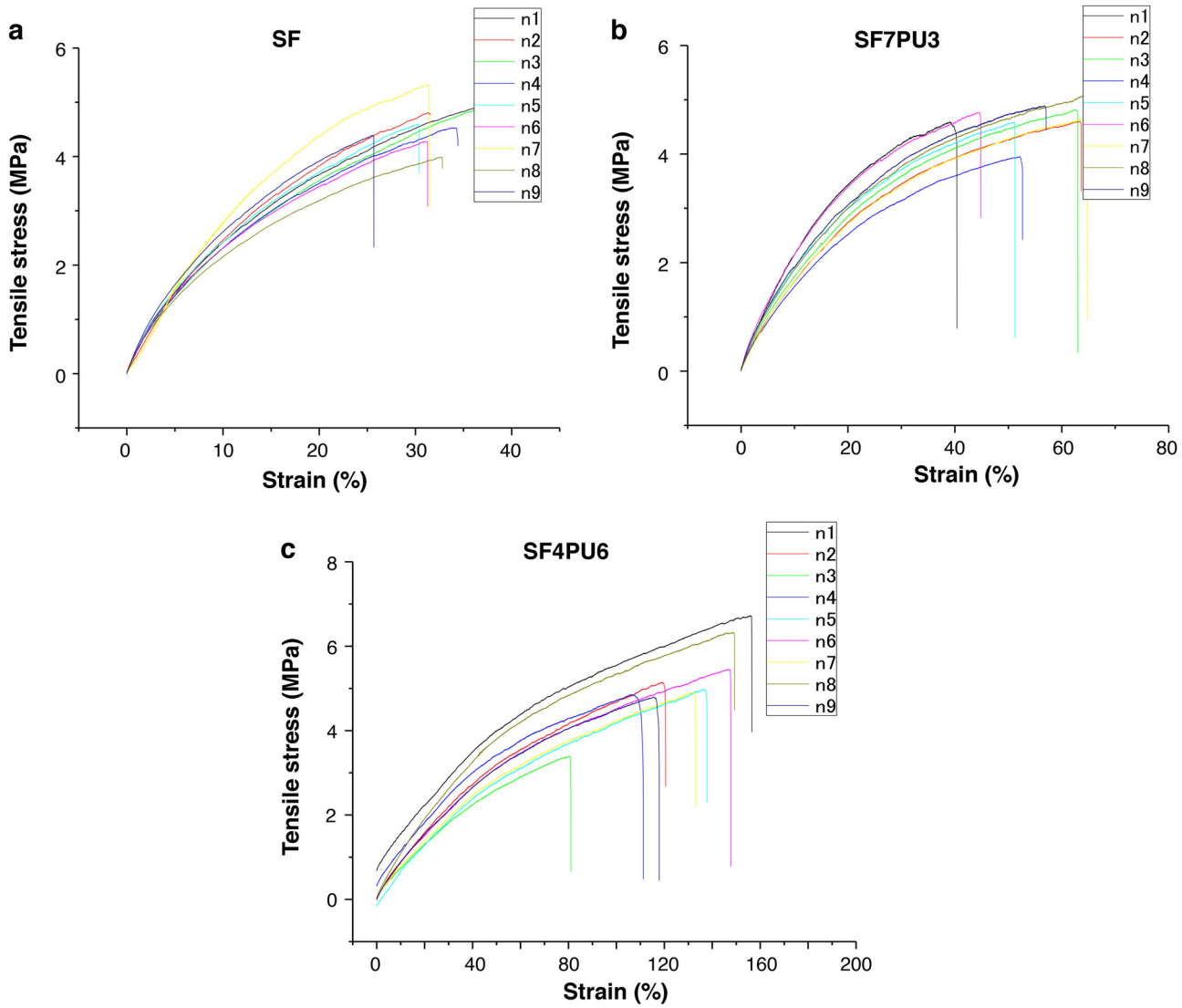

Fig. 2 Stress-strain curve of three patch types. SF **a**, SF7PU3 **b** and SF4PU6 **c**

tissue infiltration was found inside the SF7PU3 patch (Supplementary Fig. 2). At 3 months, all patch groups showed an increase of well-organized collagen formation in the neomedia layer (Supplementary Fig. 4). However, more extensive tissue infiltration inside SF7PU3 and SF patches was observed at 6 months post-implantation compared with that inside the SF4PU6 patch (Fig. 5f–h, m). EVG staining was used to assess the area of elastic fiber, which was represented by dark purple colors. One month after implantation, mature elastic fiber formation was present in all patches (Supplementary Fig. 2). Elastogenesis appeared to be progressive up to 3 months in the neomedia layer (Supplementary Fig. 4). Furthermore, the SF7PU3 patch exhibited the highest elastogenesis within the elastic lamina at 6 months (Fig. 5j–l). When the extracellular matrix of neovascular tissue was compared with native aorta, the collagen deposition was similar in organization. However, a greater quantity of collagen fibers was found in neotissue of our blend patches (Fig. 5e–h). The elastic fibers in the native aorta appeared to have an undulating pattern while those in our patches appeared straighter than normal (Fig. 5i–l). To further assess the characteristics of this straighter pattern and the density of collagen formation, long-term observation should be conducted.

Immunohistochemical staining revealed a cellular monolayer stained positively for CD31, representing endothelial cell layer formation on the luminal surface. At 1 month, the luminal surfaces of SF and SF7PU3 patches were partially covered with endothelial cells. In contrast, the SF4PU6 patch was devoid of endothelial cells (Supplementary Fig. 3). At 3 months, endothelial cells were more prominent in all patches (Supplementary Fig. 5). Almost

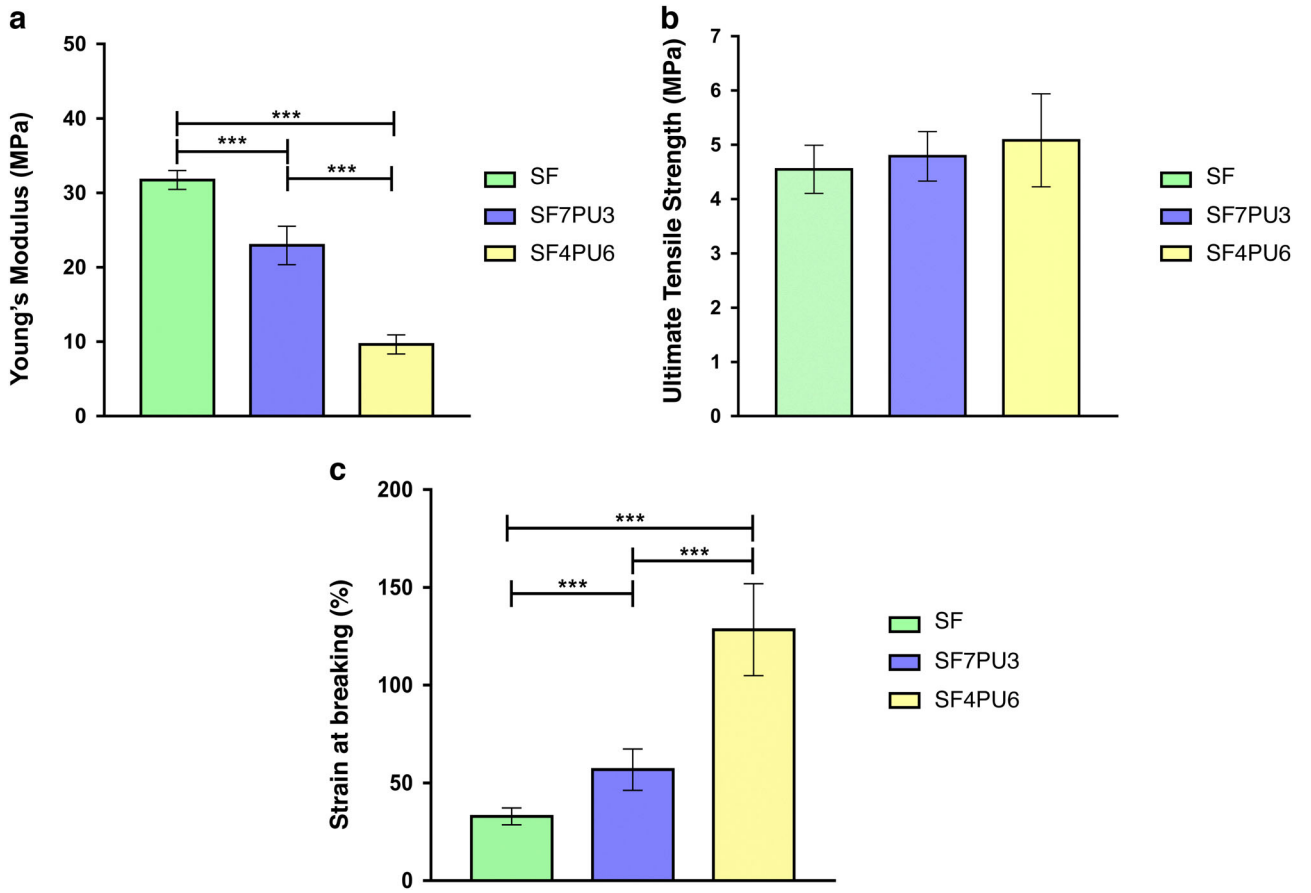

Fig. 3 Young's modulus **a**; the value in SF patch is significantly higher than the SF7PU3 and SF4PU6 patches. Ultimate tensile strength **b**; the SF patch perform the lowest tensile strength. Breaking strain **c**; the SF4PU6 patch shows the significantly highest value. Data are presented as mean ± standard error ($n = 9$) (* = $P < 0.05$, ** = $P < 0.01$ and *** = $P < 0.001$)

complete endothelialization was observed in the SF7PU3 and SF patches 6 months after implantation (Fig. 6f–g). In contrast, some parts of the luminal surface in the SF4PU6 patch were devoid of endothelial cells (Fig. 6h). In the native aorta, a confluent layer of flattened endothelial cells extended along the entire luminal surface similar to those in the SF and SF7PU3 patches (Fig. 6e–g). The α-SMA positive staining indicated smooth muscle cell (SMCs) formation. At 1 month, all patch groups showed maturity of SMCs. The multilayering of α-SMA positive cells was predominant in the neomedia (Supplementary Fig. 3). Three and six months after implantation, the thickness of SMC layers in the SF7PU3 patch resembled that of native aorta (Supplementary Fig. 3 and Fig. 6a, c). However, a thick layer of SMCs was formed in the SF and SF4PU6 patches (Fig. 6b, d). This evidence of neotissue hyperplasia may induce a stenotic problem in long-term implantation. The von Kossa staining gave no evidence of ectopic calcification in any of the patch groups throughout the study period (Fig. 6i–l). The degree of biological reactions of the three patch groups is summarized in Table 3.

Examination of target organs at 6 months post-implantation yielded no evidence of severe abnormalities that might have been caused by the implanted patches. Macroscopic and histologic observation of organs exhibited only minor changes (inflammatory infiltration of liver and kidney) in two rats from the SF group. No signs of systemic toxic effects of any patches were detected.

3.4 Imaging analysis

The results of elastogenesis, tissue infiltration, neovascular tissue thickness and endothelialization were calculated in the quantitative analyses. One month after implantation, the SF and SF7PU3 patches showed significantly higher elastogenesis compared to the SF4PU6 patch (*$P < 0.05$, **$P < 0.01$). The highest elastogenesis was observed in the SF7PU3 patch at 6 months after implantation (***$P < 0.001$) (Fig. 7a).

Concerning tissue infiltration, the SF and SF7PU3 patches exhibited significantly higher tissue infiltration compared to the SF4PU6 patch (***$P < 0.001$) throughout the

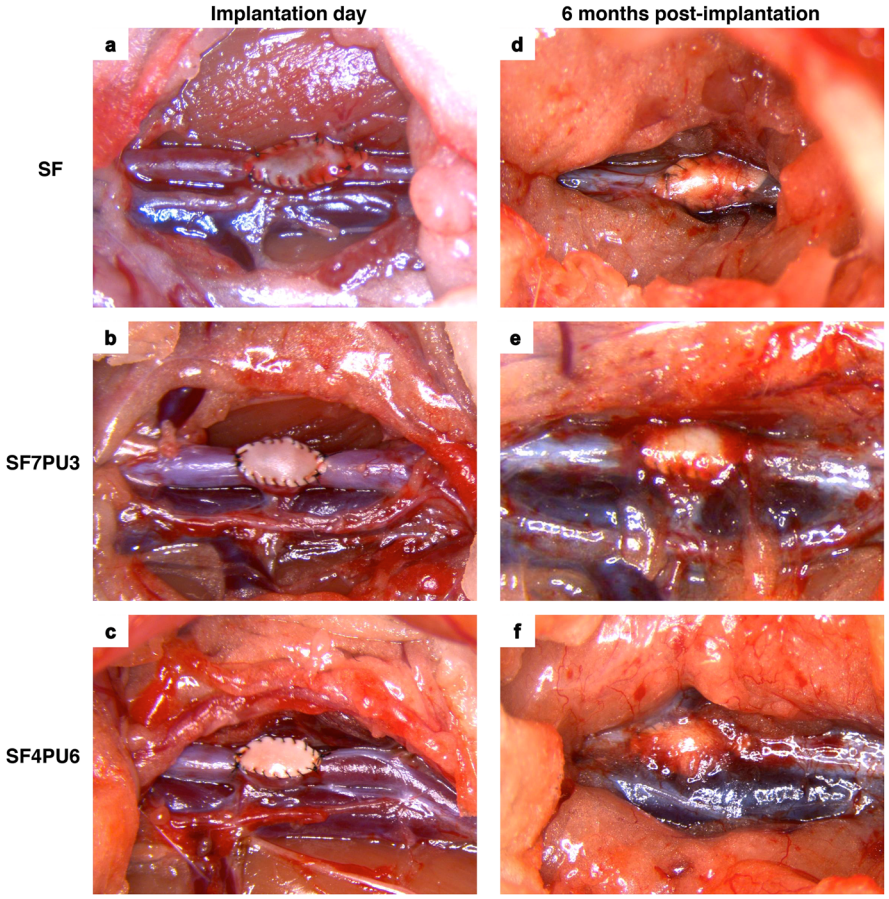

Fig. 4 The perioperative images of three types implanted patches **a–c**. There was no remarkable of blood leakage from the SF7PU3 and SF4PU6 patches **b**, **c**. The SF patch showed blood oozing at the anastomosis area **a**. After 6 months implantation, all patches were well merged with the native abdominal aorta and covered with connective tissue **d–f**

Table 3 The degree of biological reactions from three patch groups was graded from 0 to 3. Each value represents the mean ± standard error, ($n = 18$/patch types)

Patch types	Implantation time	Chronic inflammation	Foreign body reaction	Surrounding fibroconnective tissue
SF	1 month	2.33 ± 0.21	2.17 ± 0.31	1.50 ± 0.22
	3 months	1.50 ± 0.22	1.17 ± 0.17	2.17 ± 0.31
	6 months	1.33 ± 0.42	1.50 ± 0.34	2.33 ± 0.21
SF7PU3	1 month	2.17 ± 0.16	1.33 ± 0.21[a]	1.83 ± 0.31
	3 months	1.16 ± 0.30	0.50 ± 0.34 [a]	2.33 ± 0.21
	6 months	0.83 ± 0.31	0.33 ± 0.21[a]	2.17 ± 0.17
SF4PU6	1 month	2.50 ± 0.22	2.33 ± 0.21[b]	2.00 ± 0.37
	3 months	2.33 ± 0.21[a,b]	2.33 ± 0.33[a,b]	2.50 ± 0.22
	6 months	2.83 ± 0.17[a,b]	2.67 ± 0.33[a,b]	2.67 ± 0.21

[a] Compared with SF group, $P < 0.05$

[b] Compared with SF7PU3 group, $P < 0.05$

study period. At 3 and 6 months, the SF patch showed the highest tissue infiltration rates (Fig. 7c).

The neovascular tissues of SF and SF4PU6 were significantly thicker compared to the tissue of the SF7PU3 patch (**$P < 0.01$, ***$P < 0.01$) and native aorta at 1 month after implantation (***$P < 0.01$). At 3 and 6 months, the SF4PU6 patch demonstrated the highest neovascular tissue thickness. Moreover, there was no significant difference in thickness between the SF7PU3 patch and native aorta after 3 month implantation (Fig. 7b).

The endothelialization of the SF4PU6 patch was significantly less than either the SF7PU3 or the SF patches at 1, 3 and 6 months after implantation (***$P < 0.01$). In addition, the SF7PU3 and SF patches exhibited almost complete endothelialization at 6 months (Fig. 7d). Furthermore, we found a significant positive correlation

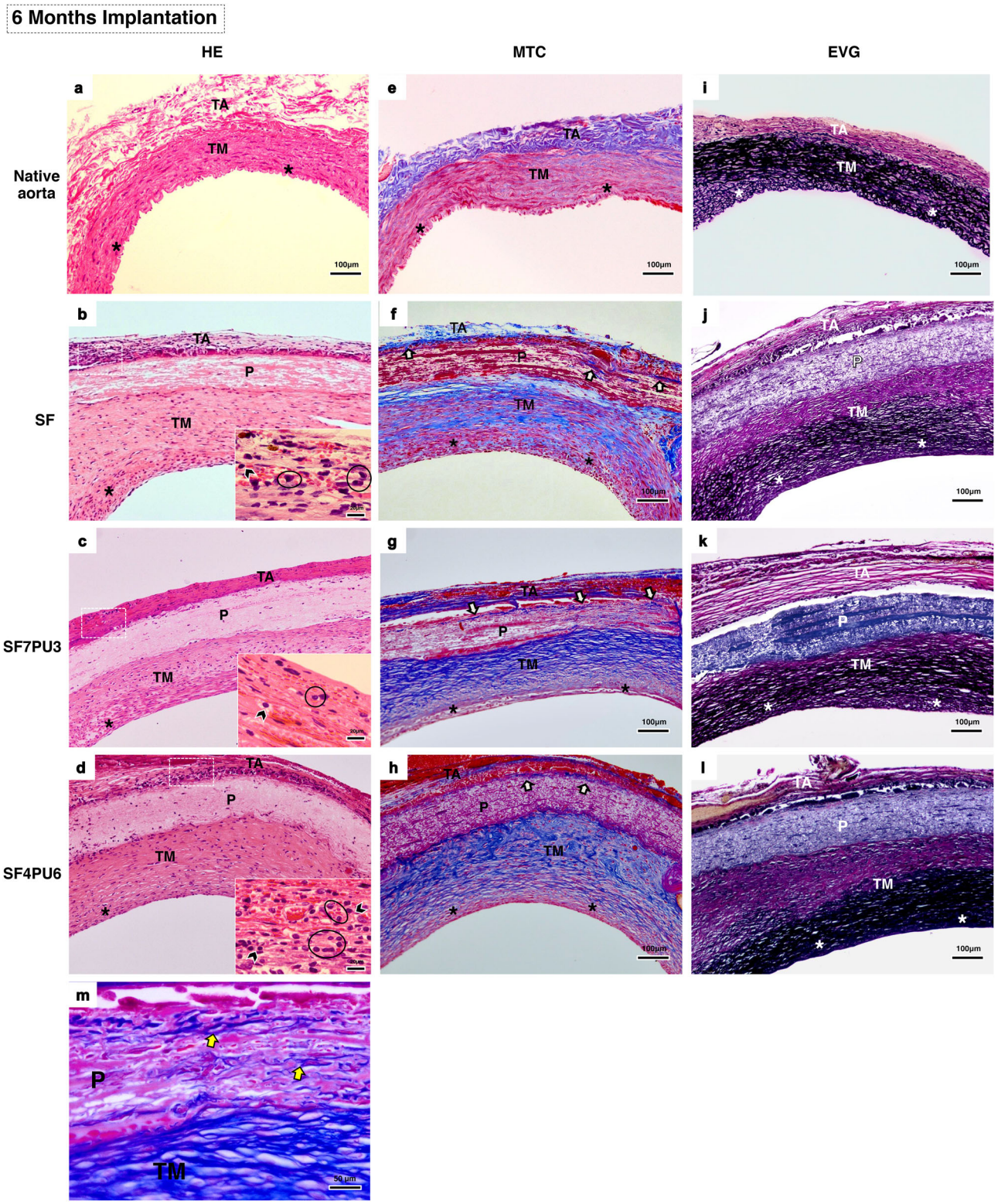

Fig. 5 Histological evaluation of neovascular tissue formation at 6 months compare with native aorta. Representative images are shown for HE staining [Native aorta **a**, SF **b**, SF7PU3 **c**, SF4PU6 **d**], MTC [Native aorta **e**, SF **f**, SF7PU3 **g**, SF4PU6 **h**], EVG [Native aorta **i**, SF **j**, SF7PU3 **k**, SF4PU6 **l**]. Higher magnification shows lymphocytes (black arrow head) are characterized by mononuclear cells with a round shape, deep basophilic and concentrically-located nucleus and plasma cells (circle) are specified by mononuclear cells, basophilic cytoplasm and an eccentric nucleus with heterochromatin in a characteristic cartwheel (inset). From MTC staining, arrow indicates tissue infiltration into the space between SF7PU3 patch fibers **m**. TA tunica adventitia, TM tunica media; Asterisk–tunica intima, P patch, Arrow –tissue infiltration

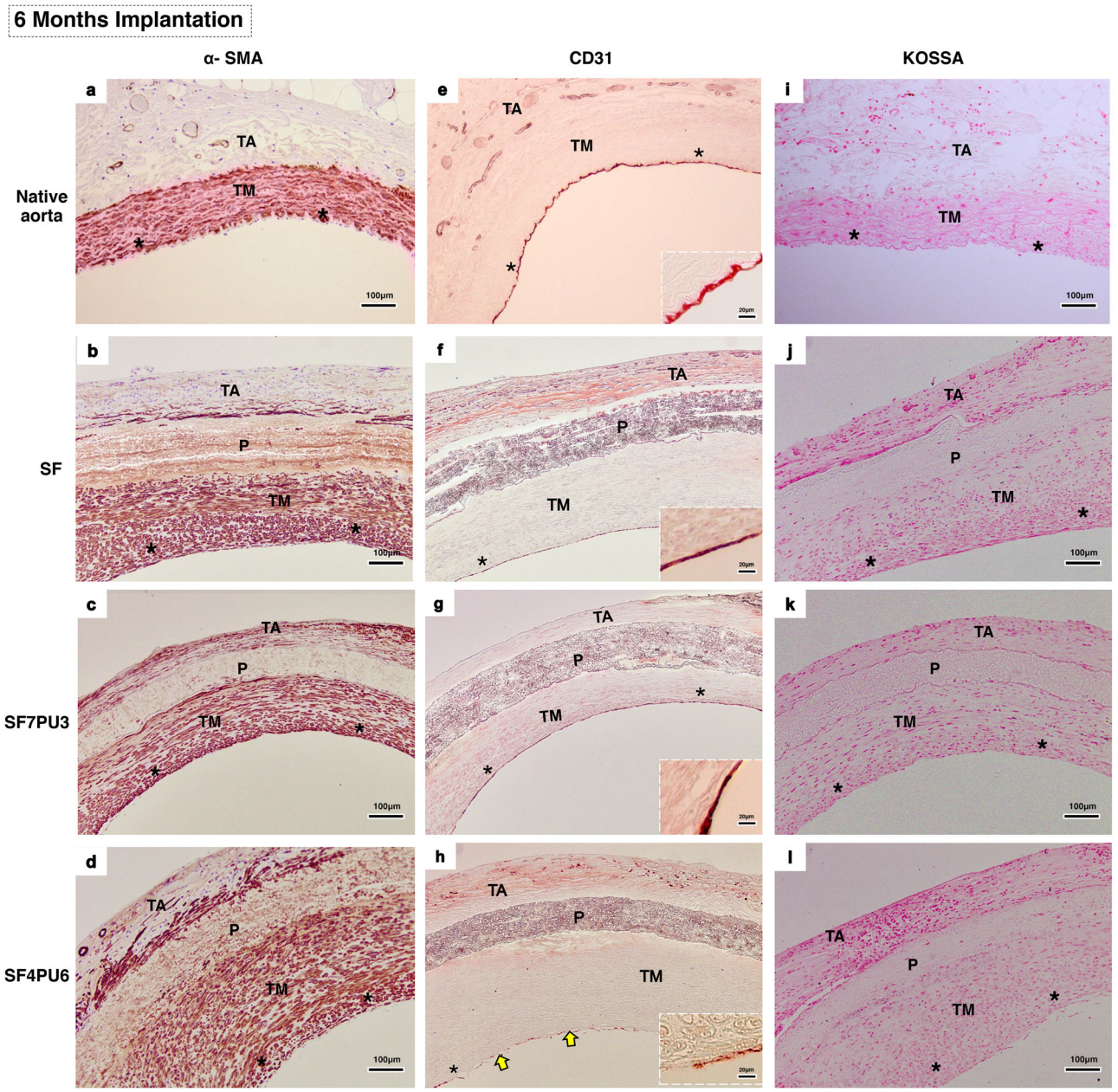

Fig. 6 At 6 months implantation, vascular smooth muscle cells and endothelial cells are detected by using α-SMA antibody [SF **b**, SF7PU3 **c**, SF4PU6 **d**] and CD31 antibody[SF **f**, SF7PU3 **g**, SF4PU6 **h**] respectively. Native aorta **a**, **e** is compared to the three patches type **b–d**, **f–h**. Higher magnification shows the morphology of endothelial cells (inset). The arrows indicate the lack of endothelial cells coverage internal lumen of the SF4PU6 patch. Von Kossa staining reveal no evidence of ectopic calcification in all patch groups [Native aorta **i**, SF **j**, SF7PU3 **k**, SF4PU6 **l**]. TA tunica adventitia, TM tunica media; Asterisk–tunica intima, P patch

between endothelialization and tissue infiltration into the patch ($R^2 = 0.7525$, $P < 0.001$) (Fig. 7e).

4 Discussion

It has become necessary to develop biopolymer-based patches that satisfy the demands of tissue engineering. These include biocompatibility, biodegradation to non-toxic products, ability to induce cell growth and proliferation, ease of handling, and good mechanical properties, as well as maintaining mechanical strength during the tissue regeneration process [25]. The physical properties of the biopolymer patch are important for scaffold characterization. A previous study demonstrated that the Poly(lactic acid) and Poly(lactic-co-glycolic acid), which have modulus of elasticity values over 1.1 GPa, are not suitable for soft tissue reconstruction [30]. The production of softer and more

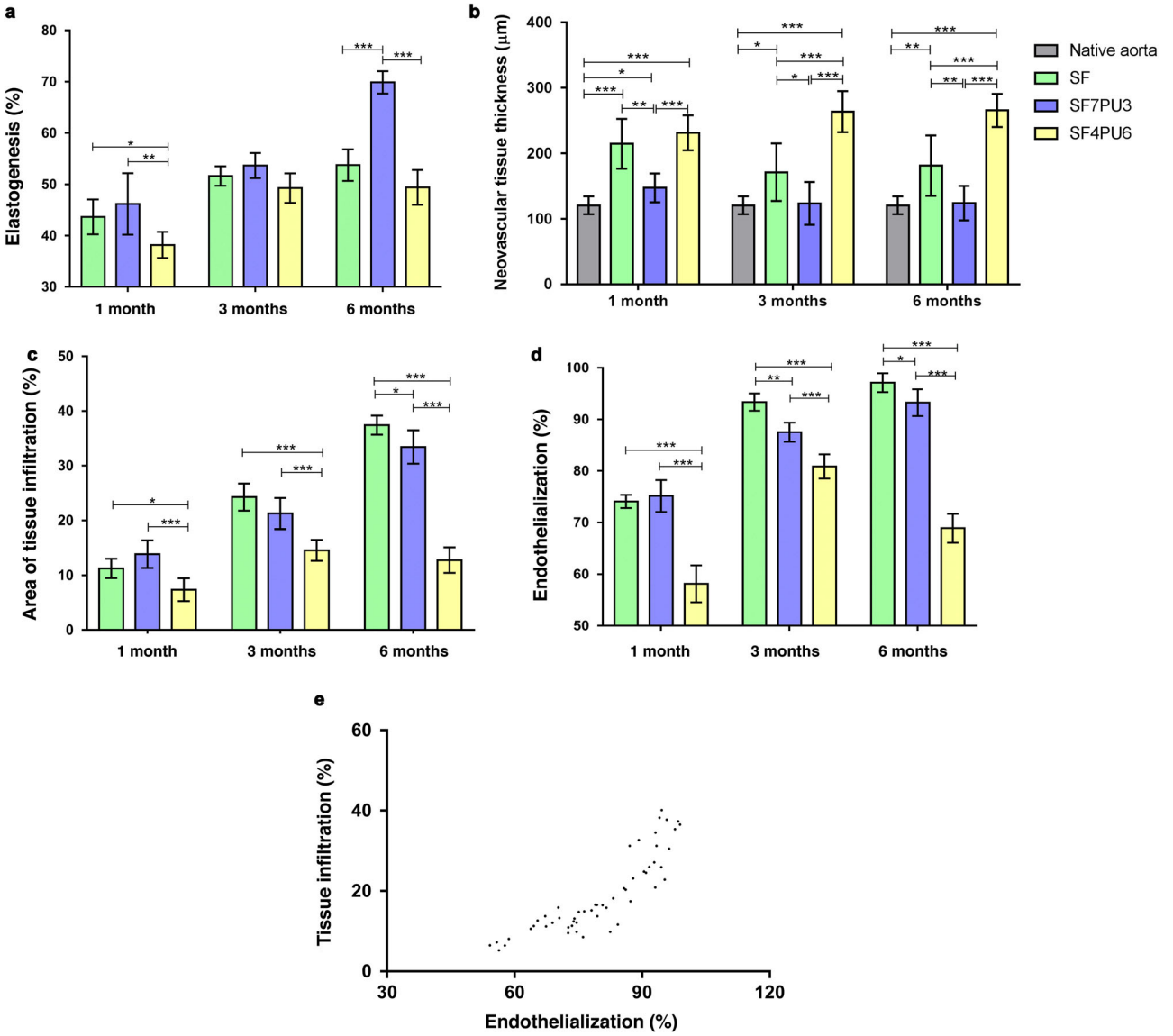

Fig. 7 The results of histopathological quantitative analyses of three types of patches. The percentage of elastic fiber formation **a**, neovascular tissue thickness **b**, tissue infiltration **c** and endothelialization **d** were evaluated at 1, 3, and 6 months after implantation. Data are presented as mean ± standard error ($n = 18$/patch types) (* = $P < 0.05$, ** = $P < 0.01$ and *** = $P < 0.001$). There was a significant positive correlation between endothelialization and tissue infiltration into the patch ($R^2 = 0.7525$, $P < 0.001$) **e**

flexible biopolymer may increase the chance for soft tissue regeneration and augmentation [25]. In this study, with increasing PU concentration, the modulus of elasticity value significantly decreased from 31.75 to 9.54 MPa. Additionally, the breaking strain of our blended patches significantly increased from 32.87% to 128.38% with decreasing silk content. This indicated that the mixture of SF and PU biopolymer was more flexible than pure SF. In this study, we expected that our SF/PU patches would replicate the mechanical properties of native blood vessel ideally to maximize patency. We found that our blended patch supported basic mechanical properties of vessel in two points. Firstly, the SF/PU patch possessed elasticity for efficient pulsatile blood flow and improved handling which helped decrease surgical time required during implantation. Nevertheless, the Young moduli of native rat abdominal aorta and human aorta are lower than our SF/PU patches [31, 32]. Therefore, in the future, we aim to improve the elasticity of patch so that it resembles that of native blood vessel. Secondly, our blended patches are able to maintain tensile strength sufficient to withstand arterial pressures without vascular rupture. The UTS of the SF/PU was greater than the UTSs of normal rat descending thoracic aorta and human ascending aorta in both circumferential and longitudinal strength [33, 34]. Therefore, the risk of vascular rupture is decreased because the mechanical

stresses acting on the vessel do not exceed the strength of the wall tissue. However, further study should concern the mechanical aspects of patches after long-term implantation. With regards to limitations of this study, we could not use pristine PU as a control because pure PU and patch blends with high PU concentrations melted and lost their structure when autoclaved. Therefore, an appropriate sterilization technique which would not affect PU structure, such as gamma radiation, should be selected.

As for biological evaluation, both SF and SF7PU3 patches revealed significantly higher tissue infiltration than the SF4PU6 patch throughout the study period. As shown in several studies, an outstanding property of SF is its ability to promote tissue infiltration, making it a promising scaffold material for tissue engineering applications [6, 12, 13]. Therefore, we hypothesized that increasing the SF content in the SF/PU patch had an effect on tissue migration. Additionally, the inflammatory response in the SF7PU3 patch also disappeared earlier and the remodeling stage was completed after 3 months. This remodeling refers to alterations in the cellular process including proper SMCs regeneration, extracellular matrix formation and endothelialization, all of which resembled that of the native vessel [35]. Generally, the tissue remodeling will be completed when the inflammatory stimulus is removed during the healing process [36]. The SF4PU6 patch manifested the highest degrees of foreign body reaction. These results seemed attributable to the higher ratio of PU. The soft segment of PU polymer is susceptible to oxidative reaction and it may contribute to the phagocytic engulfment and macrophage migration. This reaction is oxygen dependent in that superoxide anions, hydroxyl radicals and hydrogen peroxide are released by macrophage in response to the PU degradation process [36, 37]. Generally, the in vivo biocompatibility assessment involves the assessment of the presence of inflammatory cell, predominantly macrophages, since they can play a critical role in tissue healing process. Therefore, the SF7PU3 patch was characterized as the biocompatible scaffold effects that promote tissue infiltration and anti-inflammatory reaction.

SMCs are the predominant cells in the arterial wall and are essential for the structural and functional integrity of the neovessel. An appropriate migration and proliferation of SMCs is desired in our patches, aiming to obtain a wall thickness similar to that of native vessels. Several studies have shown that the excessive proliferation of SMCs, causing vascular wall thickening can lead to stenosis complications for mid- to long-term vascular graft [38, 39] and the compliance mismatch between native vessels and implanted grafts is considered one of the main causes of SMC hyperproliferation [40]. In this study, the thickness of neotissue in the media layer of the SF and the SF4PU6 patches was significantly higher than the native aorta 3 months after implantation. On the other hand, the SF7PU3 patch demonstrated wall thickness nearly that of the native aorta. We speculate that these results were due to the persistence of foreign body giant cells surrounding the SF and SF4PU6 patches. A previous study revealed that there was a positive correlation between vascular wall thickness and macrophage infiltration [41]. The excessive macrophages induced many cytokines and growth factors that facilitate vascular SMC proliferation [42]. Therefore, the inflammatory response to the implanted patch is one of the crucial factors to overcome to limit vascular stenosis and occlusion.

In vascular reconstruction, elastic fibers are the main extracellular matrix component in the arterial wall. The elastic laminae contribute to the mechanical strength, structural stability and elasticity for maintaining blood pressure with various hemodynamic stresses during the cardiac contraction [43–45]. In this study, elastic fibers were presented in all patch groups within 1 month. This is likely to due to the properties of SF which accelerate tissue remodeling at an early stage after implantation [27]. Surprisingly, elastogenesis in the SF patch was disorganized and lower than that in the SF7PU3 patch at 6 months after implantation. Theoretically, the SF patch should have had a more histotrophic character and should have induced more cell migration compared to the SF7PU3; however, the SF7PU3 patch showed more elastogenesis. It is possible that persistent of macrophage cells in the SF patch had a relationship with elastogenesis. Several studies have revealed that a chronic inflammatory response to an implanted device may interfere with tissue remodeling [36, 46]. Moreover, macrophages contain and secrete proteolytic enzymes such as elastase that could promote elastolysis and destroy the extracellular matrix [47]. Therefore, hypo-elastogenesis in vascular remodeling is considered a critical problem that reduces the strength and elasticity of the arterial wall.

After graft implantation, the considerable function of endothelium possessed anti-thrombotic activities [48]. In this study, complete endothelialization was observed in the SF7PU3 and SF patches after 6 months. Oppositely, the SF4PU6 patch revealed that some parts of luminal surface lacked endothelial cell coverage. The incomplete endothelialization may be related to less tissue infiltration into the SF4PU6 patch; in fact throughout the 6 months of vascular remodeling, we found a significant positive correlation between endothelialization and tissue infiltration into the patch ($R^2 = 0.7525$, $P < 0.001$). This hypothesis is supported by the findings of previous studies showing that tissue infiltration into a vascular graft will stimulate the settlement of endothelial cells [39, 49, 50] and that endothelialization influences vascular remodeling through cytokine secretion and growth-regulatory molecule formation to maintain the collagen basement membrane [51].

Additionally, due to the property of SF in tissue affinity, increasing the SF content in the blended SF/PU patches could be conducive to endothelialization in the early stages after implantation [27]. This finding may be a key to succeeding in the development of cardiovascular patches.

From this study, it seems that the SF7PU3 patch satisfies some requirement to develop a novel patch. These include the ability to facilitate tissue proliferation, biocompatibility and proper handling. Moreover, it showed a superior anti-calcification property when compared with commercial prosthetic patches like PTFE and PET [52–54]. However, there was no evidence of patch degradation throughout the 6 month experimental period. The long-term observation and degradation testing should be conducted. Additionally, because of moderate tissue invasion inside our blended SF/PU patches and uncertain degradation time, further studies should investigate new strategies that can accelerate the process of degradation and improve the tissue infiltration. This may be achieved by modifying the patch structure [49, 50] or bioactivating the patch through consolidation with tissue growth factor [41]. Furthermore, we hope to modify SF/PU patches for applying to the cardiac implantation model. This will be important in determining the potential of our blend SF/PU patches in cardiac function and remodeling.

5 Conclusion

In conclusion, an increase of SF concentration in the SF/PU patch had effects on the tissue infiltration, endothelialization and physical properties. Moreover, the SF7PU3 patch is the most suitable blend, based on the characteristics of sufficient practical strength and elasticity, less inflammation, proper SMC formation, complete endothelialization, high tissue infiltration and elastogenesis. Our findings demonstrate that this blended patch might be an attractive alternative in vascular reconstruction and could induce the growth of a neo-artery composed of tissue present in native healthy artery.

Acknowledgements The authors would like to thank Professor Dr. Noboru Machida and Professor Dr. Tetsuo Asakura for providing us with the histological facility and the imaging analysis system. We are also grateful to Dr. Tsunenori Kameda and Dr. Taiyo Yoshioka for providing us with the tensile testing machine. This project is entrusted to us by MAFF as part of Scientific technique research promotion program of agriculture, forestry, fishers and food industry (26051A). And, some of achievements were result from supports of grant, KAKENHI, from Grant-in-Aid for Scientific Research (15H03020) by Ministry of Education, Culture, Sports, Science and Technology Japan.

Compliance with ethical standards

Conflict of interest The authors declare that they have no competing interests.

References

1. Kazuro L, Fujimoto MD, Jianjun G, Hideki O, Tetsuro S, William RW. In vivo evaluation of a porous, elastic, biodegradable patch for reconstructive cardiac procedures. Ann Thorac Surg. 2007;83:648–54.
2. Igor T, Sava K, Tanja M, Omke T, Christoph B, Andres H, Axel H, Serghei C. Viable vascularized autologous patch for transmural myocardial reconstruction. Eur J Cardio Thorac Surg. 2009;36:306–11.
3. David K, Emile B. New Technologies for surgery of the congenital cardiac defect. Rambam Maimonides Med J. 2013;4:1–14.
4. Seokwon P, Jeffrey GJ. Biomaterials advances in patches for congenital heart defect repair. J. of Cardiovasc. Trans. Res. 2011;4:646–54.
5. Sakai T, Li RK, Weisel RD, Mickle DA, Kim ETJ, Jia ZQ, Yau TM. The fate of a tissue engineered cardiac graft in the right ventricular outflow tract of the rat. J Thorac Cardiovasc Surg. 2001;121:932–42.
6. Charu V, David LK. Silk as biomaterial. Prog. Polym. Sci. 2007;32:991–1007.
7. Altman GH, Diaz F, Jakuba C, Calabro T, Horan RL, Chen J, Lu H, Richmond J, Kaplan DL. Silk-based biomaterials. Biomaterials. 2003;24:401–16.
8. Banani K, Rangam R, Subhas CK, Xungai W. Silk fibroin biomaterials for tissue regenerations. Adv Drug Deliv Rev. 2013;65:457–70.
9. Meinel L, Kaplan D. Silk constructs for delivery of musculoskeletal therapeutics. Adv Drug Deliv Rev. 2012;12:1111–22.
10. Omenetto FG, Kaplan DL. New opportunities for ancient material. Science. 2010;329:528–31.
11. Yang M, Yamauchi K, Kurokawa M, Asakura T. Design of silk-like biomaterials inspired by mussel-adhesive protein. Tissue Eng. 2007;13:2941–7.
12. Higa K, Takeshima N, Moro F, Kawakita T, Kawashima M, Demura M, Shimazaki J, Asakura T, Tsubota K, Shimmura S. Porous silk fibroin film as a transparent carrier for cultivated corneal epithelial sheets. J Biomater Sci Polym Ed. 2011;22:2261–76.
13. Nagano A, Tanioka Y, Sakurai N, Sezutsu H, Kuboyama N, Kiba H, Tanimoto Y, Nishiyama N, Asakura T. Regeneration of the femoral epicondyle on calcium-binding silk scaffolds developed using transgenic silk fibroin produced by transgenic silkworm. Acta Biomater. 2011;7:1192–201.
14. Zhang X, Baughman CB, Kaplan DL. In vitro evaluation of electrospun silk fibroin scaffolds for vascular cell growth. Biomaterials 2008;29:2217–27.
15. Handschel J, Meyer T, Wiesmann HP. Fundamentals of tissue engineering and regenerative medicine. New York: Springer; 2009.
16. Huang FH, Sun LZ, Zheng J. In vitro and in vivo characterization of a silk fibroin-coated polyester vascular prosthesis. Artif Organs. 2008;32:932–41.
17. The Lubrizol Corporation (2017). Pellethane® TPU. (online) https://www.lubrizol.com/en/Life-Sciences/Products?Prllethane-TPU (Accessed 27 Aug 2017).
18. Pinchuk L. A review of the biostability and carcinogenicity of polyurethanes in medicine and the new generation of biostable polyurethanes. J Biomater Sci Polymer Edn. 1994;6:225–67.
19. Gunatillake PA, Adhikari R. Biodegradable synthetic polymers for tissue engineering. Eur Cell Mater. 2003;5:1–16.
20. Stokes K, Mc Venes R, Anderson JM. Polyurethane elastomer biostability. J Biomater Appl. 1995;9(4):321–54.
21. Jimenez G, Asai S, Shishido A, Sumita M. Effect of the soft segment on the fatique behavior of segmented polyurethanes. Eur Polym J. 2000;36(9):2039–50.

22. Chen JH, Wei J, Chang C, Laiw RF, Lee YD. Studies on segmented polyurethane for biomedical application: Effects of composition and hard-segment content on biocompatibility. J Biomed Mater Res A. 1998;41(4):633–48.
23. Bergmeister H, Schreiber C, Grasl C, Walter I, Plasenzotti R, Stoiber M, Schima H. Healing characteristics of electrospun polyurethane grafts with various porosities. Acta Biomater. 2013;9(4):6032–40.
24. Chiarini A, Petrini P, Bozzini S, Pra ID, Armato U. Silk fibroin/poly(carbonate)-urethane as a substrate for cell growth: in vitro interactions with human cells. Biomaterials. 2003;24:789–99.
25. Park HS, Gong MS, Park JH, Moon SI, Wall IB, Kim HW, Lee JH, Jonathan CK. Silk fibroin–polyurethane blends: Physical properties and effect of silk fibroin content on viscoelasticity, biocompatibility and myoblast differentiation. Acta Biomater. 2013;9:8962–71.
26. Scott SM, Gaddy LR, Sahmel R, Hoffman H. A collagen coated vascular prosthesis. J Cardiovasc Surg. 1987;28:498–504.
27. Fukayama T, Takagi K, Tanaka R, Hatakeyama Y, Aytemiz D, Suzuki Y, Asakura T. Biological reaction to small-diameter vascular grafts made of silk fibroin implanted in the abdominal aortae of rats. Ann Vasc Surg. 2015;29:341–52.
28. Soldani G, Losi P, Bernabei M, Burchielli S, Chiappino D, Kull S, Briganti E, Spiller D. Long term performance of small-diameter vascular grafts made of a poly(ether)urethane-polydimethylsiloxane semiinterpenetrating polymeric network. Biomaterials. 2010;31:2592–605.
29. Wu HC, Wang TW, Kang PL, Tsuang YH, Sun JS, Lin FH. Coculture of endothelial and smooth muscle cells on a collagen membrane in the development of a small-diameter vascular graft. Biomaterials. 2007;28:1385–92.
30. Ahmed M, Ramos TA, Damanik F, Le BQ, Wieringa P, Bennink M, Blitterswijk CV, Boer J, Moroni L. A combinatorial approach towards the design of nanofibrous scaffolds for chondrogenesis. Sci Rep. 2014;5:14804.
31. Assoul N, Flaud P, Chaouat M, Letourneur D, Bataille I. Mechanical properties of rat thoracic and abdominal aortas. J Biomech. 2008;41(10):2227–36.
32. Akhtar R, Sherratt MJ, Cruickshank JK, Derby B. Characterizing the elastic properties of tissue. Mater Today. 2011;14(3):96–105.
33. Abé H, Hayashi K. Data book on mechanical properties of living cells, tissues, and organs. Tokyo: Springer; 1996.
34. García-Herrera CM, Atienza JM, Rojo FJ, Claes E, Guinea GV, Celentano DJ, Burgos RL. Mechanical behaviour and rupture of normal and pathological human ascending aortic wall. Med Biol Eng Comput. 2012;50(6):559–66.
35. Renna NF, de las Heras N, Miatello RM. Pathophysiology of vascular remodeling in hypertension. Int J Hyper. 2013;2013:1–7.
36. Lamba NM, Woodhouse KA, Cooper SL. Polyurethanes Biomed Appl. CRC Press;1997. pp. 132–135.
37. Rhodes NP, Bellón JM, Buján MJ, Soldani G, Hunt JA. Inflammatory response to a novel series of siloxane-crosslinked polyurethane elastomers having controlled biodegradation. J Mater Sci Mater Med. 2005;16:1207–11.
38. Lemson MS, Tordoir JHM, Daemen MJAP, Kitslaar PJEHM. Intimal hyperplasia in vascular grafts. Eur J Vasc Endovasc Surg. 2000;19:336–50.
39. Fukayama T, Ozai Y, Shimokawadoko H, Aytemiz D, Tanaka R, Machida N, Asakura T. Effect of fibroin sponge coating on in vivo performance of knitted silk small diameter vascular grafts. Organogenesis. 2015;11:137–151.
40. Ombrellaro MP, Stevens SL, Sciarrotta J, Freeman MB, Goldman MH. Effect of endoluminal PTFE graft placement on cell proliferation, PDGF secretion, and intimal hyperplasia. J Surg Res. 1996;63:110–114.
41. Fukunishi T, Best CA, Sugiura T, Shoji T, Yi T, Udelsman B, Ohst D, Ong CS, Zhang H, Shinoka T, Breuer CK, Johnson J, Hibino N. Tissue-Engineered Small Diameter Arterial Vascular Grafts from Cell-Free Nanofiber PCL/Chitosan Scaffolds in a Sheep Model. PloS ONE. 2016;11:e0158555.
42. Danenberg HD, Welt FG, Walker M, Seifert P, Toegel GS, Edelman ER. Systemic inflammation induced by lipopolysaccharide increases neointimal formation after balloon and stent injury in rabbits. Circulation. 2002;105:2917–22.
43. Patel A, Fine B, Sandig M, Mequanint K. Elastin biosynthesis: the missing link in tissue-engineered blood vessels. Cardiovasc Res. 2006;71:40–9.
44. Faury G. Function–structure relationship of elastic arteries in evolution: from microfibrils to elastin and elastic fibres. Pathol Biol. 2001;49:310–25.
45. Long JL, Tranquillo RT. Elastic fiber production in cardiovascular tissue-equivalents. Matrix Biol. 2003;22:339–50.
46. Anidjar S, Dobrin PB, Eichorst M, Graham GP, Chejfec G. Correlation of inflammatory infiltrate with the enlargement of experimental aortic aneurysms. J Vasc Surg. 1992;16:139–47.
47. ZENA Werb, Banda, Jones MJ. PA. Degradation of connective tissue matrices by macrophages. J Exp Med. 1980;152:1537–53.
48. Pearson JD. Endothelial cell function and thrombosis. Bailieres Best Pract Res Clin Haematol. 1999;12:329–41.
49. Narayan D, Venkatraman SS. Effect of pore size and interpore distance on endothelial cell growth on polymers. J Biomed Mater Res A. 2008;87:710–8.
50. Noishiki Y, Tomizawa Y, Yamane Y, Matsumoto A. Autocrine angiogenic vascular prosthesis with bone marrow transplantation. Nat Med. 1996;2:90–3.
51. Khan OF, Sefton MV. Endothelialized biomaterials for tissue engineering applications in vivo. Trend Biotechnol. 2011;29:379–87.
52. Hayabuchi Y, Mori K, Kitagawa T, Sakata M, Kagami S. Polytetrafluoroethylene graft calcification in patients with surgically repaired congenital heart disease: evaluation using multidetector-row computed tomography. Am Heart J. 2007;153(806):e1–e8.
53. Park JC, Song MJ, Hwang YS, Suh H. Calcification comparison of polymers for vascular graft. Yonsei Med J. 2001;42:304–10.
54. Soldani G, Panol G, Sasken HF, Goddard MB, Galletti PM. Small diameter polyurethane-polydimethylsiloxane vascular prostheses made by a spraying, phase-inversion process. J Mater Sci Mater Med. 1992;3:106–13.